

# On the application of numerical analytic continuation methods to the study of quantum mechanical vibrational relaxation processes

E. Gallicchio, S. A. Egorov, and B. J. Berne

*Department of Chemistry, Columbia University, New York, New York 10027*

(Received 22 May 1998; accepted 23 July 1998)

A major problem still confronting molecular simulations is how to determine time-correlation functions of many-body quantum systems. In this paper the results of the maximum entropy (ME) and singular value decomposition (SVD) analytic continuation methods for calculating real time quantum dynamics from path integral Monte Carlo calculations of imaginary time time-correlation functions are compared with analytical results for quantum mechanical vibrational relaxation processes. This system studied is an exactly solvable system: a harmonic oscillator bilinearly coupled to a harmonic bath. The ME and SVD methods are applied to exact imaginary-time correlation functions with various level of added random noise, and also to imaginary-time data from path integral Monte Carlo (PIMC) simulations. The information gathered in the present benchmark study is valuable for the application of the analytic continuation of PIMC data to complex systems. © 1998 American Institute of Physics. [S0021-9606(98)51340-2]

## I. INTRODUCTION

The simulation of quantum dynamics in condensed phases is one of the major goals and one of the most challenging problems in computational statistical mechanics. In principle, the density matrix formalism provides all the tools necessary to study equilibrium and time-dependent properties of any physical system. In practice, however, only a few systems can be treated analytically.

Semiclassical surface-hopping techniques,<sup>1,2</sup> are often based on the assumption that only a small part of the system needs to be treated quantum mechanically. This methodology has been applied to a variety of problems ranging from spectroscopy in condensed phases,<sup>3,4</sup> proton transfer in liquids,<sup>5,6</sup> and diffusion and relaxation of excess electrons in liquids.<sup>7,8</sup> The semiclassical surface-hopping techniques are limited by the assumption that the dynamics of most of the degrees of freedom in the system can be approximated by classical mechanics. When applied to the study of quantum mechanical vibrational relaxation and vibronic transitions this assumption has been shown to produce large errors.<sup>9–11</sup> In these semiclassical methods, thermal averaging is also problematic because it may require the calculation of a large number of trajectories.

In an alternative approach, the total system is also divided into a subsystem and a bath that is treated implicitly by preaveraging over the bath degrees of freedom. This treatment leads to a reduced density matrix formalism.<sup>12</sup> The effect of the bath on the system is treated perturbatively through bath time-correlation functions. The equation of motion for the reduced density matrix is the Redfield equation.<sup>13</sup> Some of the applications to dynamical systems of interest in chemical physics range from the spin-boson problem to long range electron transfer<sup>14</sup> and vibrational relaxation.<sup>15–17</sup> In the applications the bath is still treated classically, and thus these calculations involve the same problems as discussed above.

In other studies, the calculation of dynamical quantities is attempted through brute-force calculation of real-time path integrals. This direct approach is riddled with difficulties due to the highly oscillating behavior of the integrand that introduces the so-called sign problem. Early attempts to use this approach has focused on low-dimensional problems by conditioning the integrand by working in complex time<sup>18</sup> or by introducing a filter function to preferentially sample paths close to the stationary paths.<sup>19,20</sup> Similar ideas have been successfully applied to the study of vibrational relaxation<sup>21</sup> and reactivity<sup>22</sup> in a nonadiabatic bath.

An approximate method, the centroid molecular dynamics method,<sup>23</sup> has been applied to a large variety of dynamical systems ranging from electron and proton transfer in liquids to molecular diffusion and activated dynamics in condensed phases, but its regime of validity has yet to be defined as it cannot handle quantum mechanical coherences accurately.

In this paper, quantum dynamics is simulated by performing a numerical analytic continuation of imaginary-time-correlation functions. Baym and Mermin<sup>24</sup> showed that a time-ordered quantum mechanical equilibrium correlation function is an analytic function of the time variable in the complex plane. As such, the time-correlation function calculated along the imaginary time axis (also called the Euclidean time axis) can be uniquely analytically continued to the real-time axis. This mathematical transformation, although well defined, is known to be numerically unstable and capable of enormously amplifying the unavoidable statistical and systematic errors of the imaginary-time correlation function.<sup>25</sup>

The purpose of the present study is to examine the performance of the maximum entropy (ME) and singular value decomposition (SVD) analytic continuation methods to the problem of quantum mechanical vibrational relaxation. The ME method has been successfully applied to the study of the

equilibrium dynamics of solvated electrons.<sup>26–28</sup> The SVD method has been shown to be superior to maximum entropy method in reproducing the optical spectrum of chromophore coupled to a condensed phase environment.<sup>29</sup>

A dynamical model that has been used in many contexts ranging from tunneling in Josephson junctions to activated barrier crossing, vibrational relaxation,<sup>30</sup> and vibronic absorption is that of a one-dimensional system bilinearly coupled to a harmonic bath. It has been shown that when the system is itself harmonic, the power spectra of the position and velocity, as well as the vibrational relaxation time  $T_1$  and the vibrational dephasing time  $T_2$ , are identical for fully classical and fully quantum mechanical treatments. This system thus provides one of the few analytically tractable test cases for ME and SVD methods of analytical continuation.

The one-dimensional oscillator coupled to a harmonic bath is a prototype model for studying vibrational relaxation in condensed phases, a problem that has been studied extensively classically,<sup>31</sup> with mixed quantum classical ensemble<sup>15–17</sup> and fully quantum mechanically.<sup>32,33,10</sup> These studies point out that complicated atomic and molecular systems can be approximated very well by harmonic baths. The harmonic approximation for the bath degrees of freedom allows the use of the formalism of the generalized Langevin equation in classical mechanics and of the influence functional in the quantum mechanical path integral formalism. In this study we will make the additional assumption that the tagged oscillator is harmonic. This assumption is not necessary and most of the formalism developed can be applied to an anharmonic oscillator. It allows us, however, to solve the problem analytically<sup>9</sup> at the quantum mechanical level.

The availability of analytical solutions allow to check the quality of the analytic continuation results at each stage of the calculation. This work, therefore, represents a benchmark study and paves the way for tackling more complex systems.

## II. MODEL SYSTEM

Let us consider an oscillator linearly coupled to a bath of harmonic oscillators. The Hamiltonian of the system is

$$H = H_{\text{osc.}} + H_{\text{bath}} + V_{\text{int.}}, \quad (1)$$

where  $H_{\text{osc.}}$  is the Hamiltonian of the free oscillator

$$H_{\text{osc.}} = \frac{p^2}{2m} + V(x), \quad (2)$$

where  $m$  is the reduced mass of the oscillator, and  $x$  and  $p$  are, respectively, the displacement of the oscillator from its equilibrium position and its conjugate momentum. The restoring force of the free oscillator is described by the potential  $V(x)$ . The Hamiltonian of the harmonic bath is the sum of the Hamiltonians of the component harmonic oscillators

$$H_{\text{bath}} = \sum_{\alpha} \left( \frac{p_{\alpha}^2}{2m_{\alpha}} + \frac{m_{\alpha}\omega_{\alpha}^2}{2} x_{\alpha}^2 \right), \quad (3)$$

where  $x_{\alpha}$  is the coordinate of the  $\alpha$ th oscillator,  $p_{\alpha}$  its conjugate momentum,  $\omega_{\alpha}$  its equilibrium frequency, and  $m_{\alpha}$  its reduced mass. The coupling between the oscillator and the bath is taken to be

$$V_{\text{int.}} = -x \sum_{\alpha} g_{\alpha} x_{\alpha}, \quad (4)$$

where the parameters  $g_{\alpha}$  measure the degree of coupling of the oscillator with the  $\alpha$ th normal mode of the bath.

Let us assume also that the oscillator is coupled to an external radiation through its dipole  $\mu(x) = q_0 x$  that varies linearly with the displacement coordinate  $x$ . The bath is assumed not to be directly affected by the field. We are interested in the equilibrium dynamics of the oscillator, and in particular the quantum time autocorrelation function  $\langle x(t)x(0) \rangle$  that ultimately determines the absorption of radiation by the system. The dipole absorption cross section  $\sigma(\omega)$  is, in fact, given by<sup>34</sup>

$$\sigma(\omega) = \frac{4\pi}{\hbar c} \omega (1 - e^{-\beta\hbar\omega}) I(\omega), \quad (5)$$

where the dipole spectral density  $I(\omega)$  is defined as the Fourier transform of the dipole time autocorrelation function  $q_0^2 \langle x(t)x(0) \rangle$

$$I(\omega) = q_0^2 \int_{-\infty}^{+\infty} dt e^{i\omega t} \langle x(t)x(0) \rangle. \quad (6)$$

Thus the decay time of the envelope of the position correlation function, the vibrational dephasing, or energy relaxation time is related to the broadening of the absorption band of the oscillator.

The parameter  $q_0$  trivially scales by constant the dipole correlation function and the spectral function. In the following it will be omitted to simplify the notation.

### A. Classical treatment: the generalized Langevin equation

In a classical treatment of an oscillator embedded in a bath of harmonic oscillators, the dipole absorption cross section that describes the rate of energy absorption by the oscillator from an external oscillating radiation field is

$$\sigma(\omega)^{\text{cl.}} = \frac{4\pi\beta}{c} \omega^2 C_{\mu\mu}^{\text{cl.}}(\omega), \quad (7)$$

where

$$\begin{aligned} C_{\mu\mu}^{\text{cl.}}(\omega) &= \int_{-\infty}^{+\infty} dt e^{i\omega t} \langle \mu(t)\mu(0) \rangle_{\text{cl.}} \\ &= \int_{-\infty}^{+\infty} dt e^{i\omega t} \langle x(t)x(0) \rangle_{\text{cl.}}. \end{aligned} \quad (8)$$

The autocorrelation function of the displacement of the oscillator can be obtained by solving the generalized Langevin equation<sup>35,36</sup>

$$m\ddot{x}(t) = -\frac{\partial W[x(t)]}{\partial x} + \xi(t) - \int_0^t dt' \zeta(t-t')\dot{x}(t'), \quad (9)$$

where the time-dependent friction kernel  $\zeta(t)$  is related to the spectral density of the bath modes

$$J_b(\omega) = \sum_{\alpha} \frac{g_{\alpha}^2}{2m_{\alpha}\omega_{\alpha}^2} [\delta(\omega + \omega_{\alpha}) + \delta(\omega - \omega_{\alpha})], \quad (10)$$

through a cosine transform

$$\zeta(t) = \int_{-\infty}^{+\infty} d\omega J_b(\omega) \cos(\omega t). \quad (11)$$

$W(x)$  is the potential of mean force. In the case of an harmonic bath it is given by

$$W(x) = V(x) - \frac{\zeta(0)}{2} x^2, \quad (12)$$

and  $\xi(t)$  is a Gaussian random force whose time autocorrelation function, by virtue of the fluctuation-dissipation theorem, is proportional to the friction kernel

$$\beta \langle \xi(t) \xi(0) \rangle = \zeta(t). \quad (13)$$

The generalized Langevin equation, Eq. (9), can be solved numerically<sup>31</sup> by producing a set of realizations of the random force  $\xi(t)$  compatible with Eq. (13) and integrating Eq. (9) for each realization of the random force to obtain a set of trajectories  $x(t)$ . By averaging over the trajectories, the time autocorrelation  $\langle x(t)x(0) \rangle_{\text{cl}}$  is finally recovered.

For the particular case in which the potential  $V(x)$  of the oscillator is also quadratic,  $V(x) = m\omega_0^2 x^2/2$ , a closed form for the absorption cross section can be derived<sup>36</sup>

$$\sigma(\omega) = \frac{8\pi}{mc} \frac{\omega^2 \gamma'(\omega)}{[\bar{\omega}^2 - \omega^2 + \omega \gamma''(\omega)]^2 + [\omega \gamma'(\omega)]^2}, \quad (14)$$

where  $\bar{\omega}^2 = \omega_0^2 - \zeta(0)/m$ , and  $[m\gamma'(\omega)]$  and  $[m\gamma''(\omega)]$  are, respectively, the real and imaginary parts of the complex Laplace transform of the friction kernel, namely

$$\gamma(\omega) = \gamma'(\omega) + i\gamma''(\omega) = \frac{1}{m} \int_0^{\infty} dt e^{i\omega t} \zeta(t). \quad (15)$$

It can be shown<sup>9</sup> that for a harmonic system the quantum mechanical and classical absorption cross sections coincide so that Eq. (14) is also valid when the oscillator and the bath modes are treated quantum mechanically. It follows, in particular, that the values vibrational dephasing and energy relaxation times are the same in either a classical or quantum mechanical treatment.

### III. QUANTUM TREATMENT: ANALYTIC CONTINUATION

It is extremely difficult to set up a direct numerical study of the real-time dynamics of an oscillator in a frictional bath in a quantum mechanical regime. In this paper we attempt to infer dynamical properties of the system through the analytic continuation of imaginary-time correlation functions. The legitimacy of such approach is ensured by the analyticity of quantum correlation functions.<sup>24</sup>

In particular, the real-time displacement correlation function  $\langle x(t)x(0) \rangle$ ,  $t > 0$ , in Eq. (8) can be interpreted as the complex-time displacement correlation function

$\langle x(z)x(0) \rangle$ , where  $z$  is a complex parameter, evaluated along the positive real time axis. On the same footing, the imaginary-time displacement correlation function  $\langle x(-i\tau)x(0) \rangle$ ,  $\beta\hbar > \tau > 0$ , is interpreted as the complex-time displacement correlation function evaluated along the negative imaginary-time axis. The imaginary-time and real-time correlation functions are, thus, two equivalent representations of the same analytic function. One can be converted into the other by means of the analytic continuation operation.

In performing the analytic continuation, it is useful to consider the spectral density  $I(\omega)$  of  $\langle x(t)x(0) \rangle$ . By inverting Eq. (8) and by performing the replacement  $t \rightarrow -i\tau$  (where  $t, \tau > 0$ ), we obtain

$$\langle x(-i\tau)x(0) \rangle = \frac{1}{2\pi} \int_{-\infty}^{+\infty} d\omega e^{-\omega\tau} I(\omega), \quad (16)$$

The imaginary-time correlation function  $\langle x(-i\tau)x(0) \rangle$  is, thus, the Fourier-Laplace transform of  $I(\omega)$ . Assuming  $\langle x(-i\tau)x(0) \rangle$  is known for  $0 < \tau < \beta\hbar$ , the inversion of the integral equation (16) effectively completes the analytic continuation because  $\langle x(t)x(0) \rangle$  is obtainable for real and positive  $t$  by a straightforward back Fourier transformation of  $I(\omega)$

$$\langle x(t)x(0) \rangle = \frac{1}{2\pi} \int_{-\infty}^{+\infty} d\omega e^{-i\omega t} I(\omega). \quad (17)$$

It is convenient to perform the analytic continuation starting from the displacement imaginary-time correlation function of the position  $R^2(-i\tau) = \langle |x(-i\tau) - x(0)|^2 \rangle$ . In terms of  $R^2(-i\tau)$  and the dipole absorption cross section  $\sigma(\omega)$ , Eq. (16) becomes

$$R^2(-i\tau) = \langle |x(-i\tau) - x(0)|^2 \rangle = \int_0^{+\infty} d\omega \sigma(\omega) K(\omega, \tau), \quad (18)$$

where the kernel function  $K(\omega, \tau)$  is

$$K(\omega, \tau) = \frac{\hbar c}{4\pi^2} \frac{\cosh\left[\frac{\beta\hbar\omega}{2}\right] - \cosh\left[\beta\hbar\omega\left(\frac{1}{2} - \frac{\tau}{\beta\hbar}\right)\right]}{\omega \sinh\left(\frac{\beta\hbar\omega}{2}\right)}, \quad (19)$$

and the detailed balance relation  $I(-\omega) = e^{-\beta\hbar\omega} I(\omega)$  has been used. The corresponding equation for  $\langle |x(t) - x(0)|^2 \rangle$  can be easily derived by expressing Eqs. (18) and (19) in real time

$$\begin{aligned} R^2(t) &= \langle |x(t) - x(0)|^2 \rangle \\ &= \frac{\hbar c}{4\pi^2} \int_0^{+\infty} d\omega \sigma(\omega) \frac{1 - \cos(\omega t)}{\omega \tanh(\beta\hbar\omega/2)}. \end{aligned} \quad (20)$$

By differentiating twice Eq. (20) a relation between the real part of  $\langle \dot{x}(t)\dot{x}(0) \rangle = \langle \mathbf{v}(t) \cdot \mathbf{v} \rangle$  and  $\sigma(\omega)$  is obtained

$$\frac{8\pi^2 q^2}{\hbar c} \text{Re}[\langle \mathbf{v}(t) \cdot \mathbf{v} \rangle] = \int_0^{\hbar} d\omega \omega \sigma(\omega) \frac{\omega \cos \omega t}{\tanh \beta\hbar\omega/2}. \quad (21)$$

The imaginary-time correlation functions are readily available from path integral Monte Carlo (PIMC) simulations. The analytic continuation approach, therefore, has the clear advantage of avoiding the difficult task of following the dynamics of the system in real time. It suffers, however, from the fact that numerical analytic continuation is an ill-conditioned problem. In general, changes in the model system parameters produce small variations in the imaginary-time correlation functions but much larger variations in the real-time correlation functions. This means that by inverting Eq. (18) even extremely small statistical noise present in the imaginary-time correlation function can be amplified to such an extent that little can be said about the real-time dynamics of the system. By correctly handling of the statistical noise we can, at least, successfully identify those features of the absorption spectrum and of the real-time correlation function that are less affected by the statistical noise.

#### IV. MAXIMUM ENTROPY

The maximum entropy method (MEM) ensures proper handling of the statistical noise in the inversion of Eq. (18). The method makes use of *a priori* knowledge about the system to determine those features of the real-time correlation function that are not constrained by the noisy imaginary-time correlation function. For example, the method automatically incorporates the property of positiveness of the absorption spectrum.

The following is a brief description of the implementation of the maximum entropy inversion method. The justification of the method<sup>37,38</sup> and the details of our implementation<sup>27,28</sup> have been previously reported.

To numerically invert Eq. (25), the frequency axis is discretized on a grid  $\{\omega_j, j=1, \dots, N\}$ . A  $N$ -dimensional vector  $\mathbf{A}$ , called the *map*, is then defined having elements

$$A_j = \sigma(\omega_j) \Delta \omega_j, \quad j=1, \dots, N, \quad (22)$$

which represent the integrated values of the, still unknown, absorption spectrum in each grid spacing  $j$  of size  $\Delta \omega_j$ .

The input of the inversion procedure is the set of the  $M$  calculated values of the displacement imaginary-time correlation function  $D_i = \langle |x(-i\tau_i) - x(0)|^2 \rangle$  at the imaginary times  $\{\tau_i, i=1, \dots, M\}$ .

With the frequency and imaginary-time discretizations given above, Eq. (18) assumes the form

$$\mathbf{D} = \mathbf{K}\mathbf{A}, \quad (23)$$

where  $\mathbf{A}$  and  $\mathbf{D}$  are vectors with components  $A_j$  and  $D_i$ , respectively, and the kernel matrix  $K$ , defined as  $K_{ij} = K(\tau_i, \omega_j)$  [see Eq. (19)], describes a linear transformation from the  $N$ -dimensional map space to the  $M$ -dimensional data space. Given a trial map  $\mathbf{A}$ , we define a measure of the fit between  $\mathbf{K}\mathbf{A}$  and  $\mathbf{D}$

$$\chi^2(\mathbf{A}) = \sum_i^M \frac{[D_i - (\mathbf{K}\mathbf{A})_i]^2}{\sigma_i^2}, \quad (24)$$

where the  $\sigma_i$ 's are the uncertainties associated with the calculated imaginary-time data  $D_i$ .

Because of the unavoidable uncertainty on the data, it is not advisable to seek a perfect fit to the data by minimizing  $\chi^2(\mathbf{A})$ . The maximum entropy method, instead, introduces a regularizing function, called the entropy, and inverts Eq. (18) by maximizing the function

$$Q(\mathbf{A}) = \alpha S(\mathbf{A}) - \chi^2(\mathbf{A})/2. \quad (25)$$

The entropy function  $S(\mathbf{A})$  is defined as

$$S = \sum_{j=1}^N \left[ A_j - m_j - A_j \ln \frac{A_j}{m_j} \right], \quad (26)$$

where  $m_j$ 's are positive parameters derived in analogy with Eq. (22) from the so-called *default* map  $m(\omega)$ . The unconstrained maximum of the entropy occurs at  $\hat{A}_i = m_i$  for which  $\hat{S} = 0$ . The default map  $m(\omega)$  is chosen to be consistent with any prior information about the map that is available. A default map for the present study has been derived using known sum rules of the dipole absorption spectrum as previously reported.<sup>27</sup> The form (26) for the entropy has been shown to be the most general form consistent with the axioms of the MEM formalism.<sup>38</sup>

The arbitrary parameter  $\alpha$  in Eq. (25) is interpreted as the inverse Lagrange multiplier in the constrained maximization of  $S$  with a fixed value of  $\chi^2$ . It basically weighs the importance of the entropy function over the  $\chi^2$  function in determining the outcome of the maximum entropy inversion. In this paper this Lagrange multiplier is selected according to the classic maximum entropy<sup>38,39</sup> scheme in which the Lagrange multiplier is determined self-consistently. The method, thus, has no adjustable parameters.

#### V. SINGULAR VALUE DECOMPOSITION METHOD

As an alternative to the maximum entropy analytic continuation method, we consider the approach based on the singular value decomposition (SVD).<sup>29,40</sup> The application of the SVD method for inverting the imaginary-time data has been discussed in some detail in Ref. 29; here we present a brief summary.

Introducing the transpose,  $K^T$ , of the kernel matrix  $K$ , Eq. (23) can be inverted in the following matrix form:

$$\mathbf{A} = (\mathbf{K}^T \mathbf{K})^{-1} \mathbf{K}^T \mathbf{D}. \quad (27)$$

In view of the ill-posed nature of the analytic continuation problem, the matrix  $\mathbf{K}^T \mathbf{K}$  is nearly singular, and in order to compute its inverse one has to resort to the SVD method.<sup>41</sup> The smallest eigenvalues of this matrix will greatly amplify any statistical noise inherent in  $\mathbf{D}$ . Therefore we introduce a cutoff by setting to zero all eigenvalues  $\lambda_k$  for which the ratio  $\lambda_k / \lambda_{\max}$  is smaller than the statistical error in  $\mathbf{D}$  ( $\lambda_{\max}$  is the largest eigenvalue of  $\mathbf{K}^T \mathbf{K}$ ).

An additional problem in applying the SVD method to the inversion of the imaginary time data stems from the fact that the SVD by itself (unlike the maximum entropy method) does not guarantee the positivity of the calculated spectrum.<sup>29,40</sup> In Ref. 29, this problem was circumvented by reconstructing the *difference* between the quantum mechanical and the (known) classical spectrum, rather than the quantum spectrum itself. This difference can alternate in sign,

which makes it possible to apply the SVD method without imposing the ‘‘positivity constraint.’’ However, in the present problem the quantum and classical spectra are identical, and the above approach has no meaning. Moreover, the classical result is not always known. We have employed a ‘‘triangular window’’<sup>42</sup> which ensures the positivity of the solution (at least in the absence of noise), but concomitantly reduces the resolution, as indeed we will see below. Specifically, the application of triangular window amounts to replacing the eigenvalue  $\lambda_i$  with  $\lambda_i/(1-(i-1)/k_{\min})$ , where the index  $k_{\min}$  corresponds to the smallest eigenvalue which remained after introducing the cutoff based on the statistical error in  $\mathbf{D}$ .

We close this section by noting that for anharmonic systems the SVD method can be applied in the same form as in Ref. 29 by reconstructing the difference between the quantum mechanical spectrum and the one obtained from centroid molecular dynamics.

## VI. PIMC

For a system composed of a single particle of mass  $m$  interacting with a potential  $V(\mathbf{r})$ , the quantum average of an position dependent observable is expressed in the path integral representation<sup>43</sup>

$$\langle O \rangle = \frac{\oint \mathcal{D}\mathbf{r}(\cdot) O[\mathbf{r}(\cdot)] e^{-S[\mathbf{r}(\cdot)]/\hbar}}{\oint \mathcal{D}\mathbf{r}(\cdot) e^{-S[\mathbf{r}(\cdot)]/\hbar}}, \quad (28)$$

where the symbol  $\oint \mathcal{D}\mathbf{r}(\cdot)$ , the functional *path integral*, represents the sum over all possible closed paths  $\mathbf{r}(\cdot)$ ,  $O[\mathbf{r}(\cdot)]$  is the functional representing the space-dependent quantum observable  $O$

$$\langle \mathbf{r} | O | \mathbf{r}' \rangle = O(\mathbf{r}) \delta(\mathbf{r} - \mathbf{r}') \quad (29)$$

and the Euclidean-time action  $S$  is the functional of the path  $\mathbf{r}(\cdot)$  parameterized by the imaginary-time (or Euclidean-time) parameter  $\tau$ ,  $0 < \tau < \beta\hbar$ ,

$$S[\mathbf{r}(\cdot)] = \int_0^{\beta\hbar} d\tau \left[ \frac{m}{2} \left| \dot{\mathbf{r}}(\tau) \right|^2 + V[\mathbf{r}(\tau)] \right]. \quad (30)$$

For the Hamiltonian defined by Eqs. (1) to (4) the Euclidean-time path integral is performed over all possible paths in imaginary time of the displacement of the tagged oscillator and of all the bath modes. The integrals over the paths of the harmonic modes of the bath, involving a quadratic action, can be evaluated analytically, giving rise to nonlocal contributions to the action in the form of an *influence functional*<sup>43,44</sup>

$$S_I[x(\cdot)] = -\frac{\beta\hbar}{2} \int_0^{\beta\hbar} \frac{d\tau}{\beta\hbar} \int_0^{\beta\hbar} \frac{d\tau'}{\beta\hbar} x(\tau) \Gamma(\tau - \tau') x(\tau'), \quad (31)$$

where the function  $\Gamma(\tau)$  plays a similar role to the time-dependent friction kernel in the classical treatment by the generalized Langevin equation (GLE) and is given by

$$\Gamma(\tau) = \beta\hbar \int_0^\infty d\omega J_b(\omega) \frac{\omega \cosh[\beta\hbar\omega(1/2 - \tau/\beta\hbar)]}{\sinh(\beta\hbar\omega/2)}. \quad (32)$$

Here  $J_b(\omega)$  is the spectral density of the bath modes defined in Eq. (10), and is a property depending on the frequencies and coupling strengths of the bath and not on whether or not the bath is classical or quantum mechanical.  $J_b(\omega)$  will be the same for the the classical and quantum mechanical calculations.<sup>9</sup>

The total action is obtained by adding the influence functional (31) to the frictionless action in Eq. (30)

$$S[x(\cdot)] = \int_0^{\beta\hbar} d\tau \left[ \frac{m}{2} \left| \dot{x}(\tau) \right|^2 + V[x(\tau)] \right] + S_I[x(\cdot)]. \quad (33)$$

Equilibrium averages are given by expressions similar to Eq. (28).

For numerical computations the path integral is discretized.<sup>18</sup> The functional integral is replaced by a multi-dimensional integral on the discrete set of variables  $\{x_j, j = 1, \dots, p\}$  that describe the discretized path in imaginary time. In the primitive form,<sup>45</sup> the action from Eq. (33) assumes the discretized form

$$S = \frac{mp}{2\beta\hbar} \sum_{j=1}^p (x_j - x_{j+1})^2 + \frac{\beta\hbar}{p} \sum_{j=1}^p V(x_j) - \frac{\beta\hbar}{2p^2} \sum_{j,j'=1}^p x_j \Gamma_{j-j'} x_{j'}, \quad (34)$$

where  $\Gamma_{j-j'} = \Gamma(\tau_j - \tau_{j'})$ .

In the particular case where  $V(x) = m\omega_0^2 x^2/2$ , the exact action (33) can be diagonalized by working in the Fourier representation. The result is

$$S[\{\hat{x}_n\}] = -\beta\hbar \left[ \frac{1}{2} (m\omega_0^2 - \hat{\Gamma}'_0) \hat{x}_0^2 + \sum_{n=1}^\infty (m\Omega_n^2 + m\omega_0^2 - \hat{\Gamma}'_n) |\hat{x}_n|^2 \right], \quad (35)$$

where  $\Omega_n = 2\pi n/\beta\hbar$ ,

$$\hat{\Gamma}'_n = 2 \int_0^{\beta\hbar/2} \frac{d\tau}{\beta\hbar} \Gamma(\tau) \cos(\Omega_n \tau), \quad (36)$$

and

$$\hat{x}_n = \int_0^{\beta\hbar} \frac{d\tau}{\beta\hbar} x(\tau) e^{i\Omega_n \tau}. \quad (37)$$

The path integral is expressed as an integral over the new complex variables  $\{\hat{x}_n\}$  so that the integration over a continuous path is replaced by the integration over an infinite number of variables. In Eq. (35) the coupling terms between different variables are absent so that the path integral can be calculated analytically by solving the resulting Gaussian integrals. By inspection we see that  $\langle \hat{x}_n \rangle = 0$  and

$$\langle \hat{x}_0^2 \rangle = \frac{1}{\beta m \omega_0^2 - \bar{\Gamma}'_0},$$

$$\langle |\bar{x}_n|^2 \rangle = \frac{1}{\beta(m\Omega_n^2 + m\omega_0^2 - \bar{\Gamma}'_n)}, \quad n \neq 0. \quad (38)$$

The average of many observables can be obtained analytically using the results above. For example, the imaginary-time displacement correlation function can be expressed in terms of the Fourier coefficients

$$R^2(-i\tau) = \langle |x(-i\tau) - x(0)|^2 \rangle$$

$$= \sum_{n=1}^{\infty} 4 \langle |\hat{x}_n|^2 \rangle [1 - \cos(\Omega_n \tau)]. \quad (39)$$

Inserting Eq. (38) in Eq. (39), we can express the exact imaginary-time displacement correlation function of a harmonic oscillator in a bath of harmonic oscillators as an infinite series of terms that can be computed analytically.

It is useful to derive an analytic expression for the solution of the discretized path integral with the action given in Eq. (34) for an harmonic oscillator. In this case we perform the change of variables

$$x_j = \sum_{k=0}^{p-1} q_k e^{-i2\pi k(j-1)/p}. \quad (40)$$

In the new variables  $q_k = q_{p-k}^*$  the action becomes diagonal and the discretized path integral can be again computed analytically by solving the resulting Gaussian integrals. The result for the imaginary-time displacement correlation function is

$$R^2[-i(j\beta\hbar/p)]_{(p)}$$

$$= \frac{2\beta\hbar^2[1 - (-1)^j]}{m[2p^2 + (\beta\hbar\omega)^2 - \bar{\Gamma}'_0]}$$

$$+ \sum_{k=1}^{p/2-1} \frac{4\beta\hbar^2[1 - \cos(2\pi k j/p)]}{m\{2p^2[1 - \cos(2\pi k/p)] + (\beta\hbar\omega)^2 - \bar{\Gamma}'_k\}}, \quad (41)$$

where  $j=0, \dots, p/2$  and  $\bar{\Gamma}'_k$  is the cosine transform of  $\Gamma_j$ .

Even though Eq. (39) gives an analytic expression for the imaginary-time displacement correlation function, its analytic continuation to real time cannot be performed by simply replacing  $\tau$  with  $it$  because the infinite series must be first summed and written in a closed form. As anticipated, however, the result for the absorption cross section coincides with the one [Eq. (14)] presented for the classical case.

For the discretized form (41) the direct analytic continuation is mathematically undefined because the imaginary-time correlation function is known only on a finite set of points. We cannot, therefore, write down an expression for the absorption cross section for finite  $p$ . In this case, however, the maximum entropy analytic continuation is still well

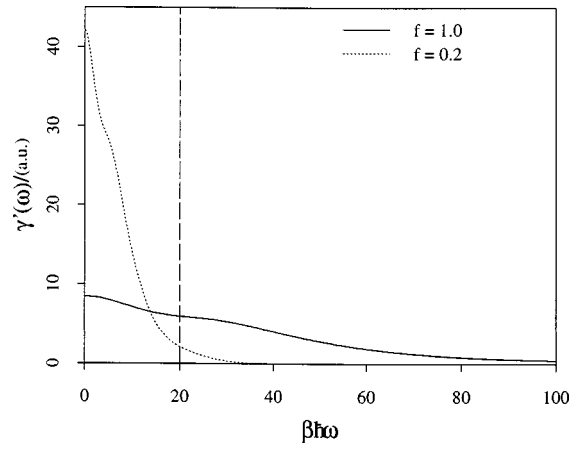


FIG. 1. The real part of the complex Laplace transform of the dynamical friction kernel of the harmonic oscillator linearly coupled to a bath of harmonic oscillators for two values of the parameter  $f$  [see Eq. (42)]. The position of the vertical dashed line corresponds to the frequency of the tagged oscillator.

defined if random noise (of amplitude that can be made very small) is superimposed on the imaginary-time data.

In the next section we present the application of the maximum entropy method to the calculation of the absorption spectrum and real-time velocity correlation function of a harmonic oscillator coupled linearly to a bath of harmonic oscillators.

## VII. RESULTS AND DISCUSSIONS

We have considered an harmonic oscillator of frequency  $\omega_0 = 20$  a.u. and mass  $m = 1$  a.u. at the inverse temperature  $\beta = 1$  a.u. The properties of the bath are characterized by the spectral density of bath modes  $J_b(\omega)$  or, equivalently, by the classical dynamical friction kernel  $\zeta(t)$ . For this study we take

$$\zeta(t) = \zeta_0 \{ e^{-\alpha_1(ft)} [1 + a_1(ft)^4] + a_2(ft)^4 e^{-\alpha_2(ft)^2} \}, \quad (42)$$

a form that resembles the dynamical friction kernel of an oscillator in a fluid of Lennard-Jones particles.<sup>46</sup> In atomic units,  $\zeta_0 = 225$ ,  $a_1 = 1.486 \times 10^5$ ,  $a_2 = 285$ ,  $\alpha_1 = 903$ ,  $\alpha_2 = 75.0$ , and the parameter  $f$  assumes, in the two cases examined, the values  $f = 1$  and  $f = 0.2$ . The real part of the complex Laplace transform of the dynamical friction kernel  $\gamma'(\omega)$ , proportional to the spectral density of bath modes  $J_b(\omega)$ , is shown in Fig. 1 for the two values of  $f$ .

In Fig. 1 we show by a vertical dashed line the frequency  $\omega_0$  of the tagged oscillator. The decay rate of the amplitude of the oscillations of the tagged oscillator due to the interaction with the bath is measured qualitatively by the value of  $\gamma'(\omega)$  at  $\omega_0$ . The exact absorption cross sections and the exact velocity correlation functions of the tagged oscillator are given by Eq. (14) and Eq. (21) and are shown in Fig. 2. In agreement with the fact that  $\gamma'(\omega_0)$  for  $f = 1$  is larger than  $\gamma'(\omega_0)$  for  $f = 0.2$ , we find that the velocity correlation function of the oscillator decays more rapidly for  $f = 1$ . Correspondingly, the absorption band for  $f = 0.2$  is narrower than the one obtained for  $f = 1$ . By considering the difference

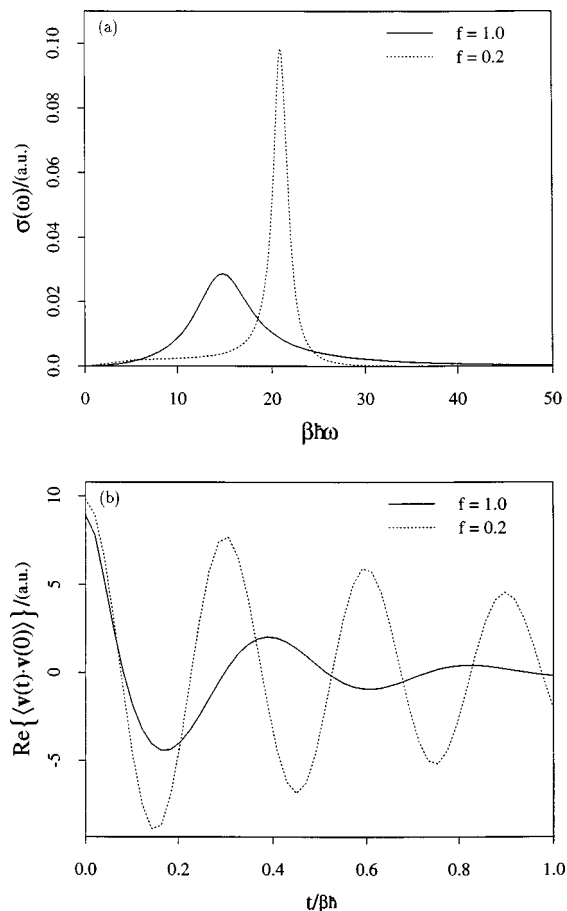


FIG. 2. (a) The exact absorption cross section and (b) the real part of the exact velocity correlation function of the harmonic oscillator linearly coupled to a bath of harmonic oscillators for two values of the parameter  $f$  [see Eq. (42)].

in the rate of decay of the velocity correlation functions, in the following the  $f=1$  case will be referred as the “high damping” case and the the  $f=0.2$  case as the “low damping” case.

### A. Maximum entropy inversion

In the remainder of this section we will address the problem of reproducing the exact absorption spectra and the velocity correlation functions, shown in Fig. 2, by maximum entropy analytic continuation of the imaginary-time displacement correlation functions generated numerically by PIMC simulations. We will also present details of the simulations and of the maximum entropy inversions to discuss the origin of the observed deviations from the exact results.

Three possible sources of imaginary-time data are available and each of them enables us to probe a different aspect of the errors involved in the maximum entropy analytic continuation.

We will first consider the imaginary-time displacement correlation function data obtained by inserting the exact absorption cross section (14) in Eq. (18) and integrating numerically using the same integration rule and frequency grid used in the maximum entropy inversion. By adding some random noise on the data so generated, and using them as input for the maximum entropy analytic continuation, we can

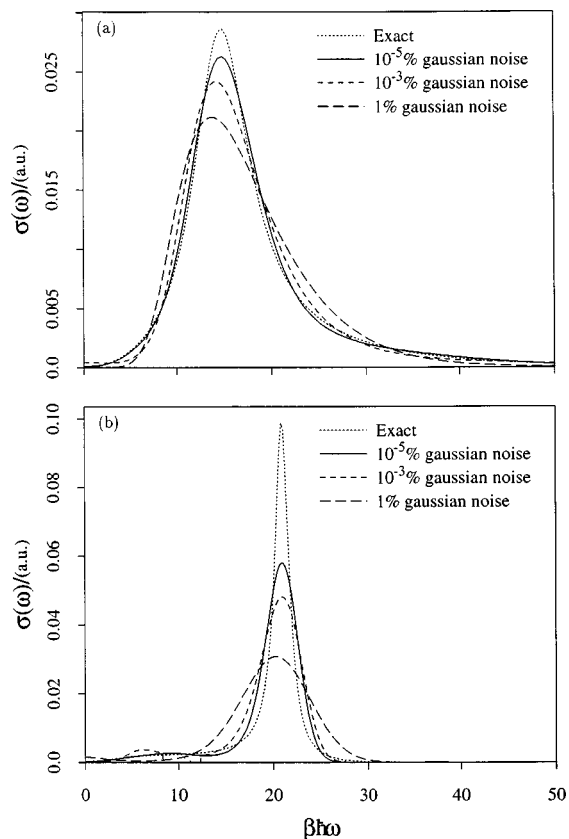


FIG. 3. The absorption cross section of the harmonic oscillator linearly coupled to a bath of harmonic oscillators for (a)  $f=1$  and (b)  $f=0.2$ , calculated by maximum entropy inversion of the exact imaginary-time displacement correlation functions to which a specified amount of Gaussian random noise has been added, compared with the exact absorption spectra from Fig. 2(a).

study how the absorption spectrum and the velocity correlation function change as the amplitude of the artificially added noise is decreased. This study should probe the bias on the solution introduced by the numerical maximum entropy analytic continuation method, i.e., the effect of the imaginary-time and frequency discretization and the effect of performing the computations using the finite arithmetics of a computer.

In Fig. 3 we show the absorption spectra obtained as described above by decreasing the relative amplitude of the random noise from 1% to  $10^{-5}\%$  (corresponding to simulated data with 2 to 7 significant figures) compared with the exact absorption spectra. The corresponding real-time velocity correlation functions are shown in Fig. 4. The exact imaginary-time data are calculated on the imaginary time grid  $\tau_j = j\beta\hbar/256$  for  $j = 1, \dots, 128$ , and the frequency grid for the calculation of the absorption spectra is composed of 250 points on the interval  $0 < \omega < 50$  a.u. for the low damping case and  $0 < \omega < 100$  a.u. for the high damping case.

We see that in the low damping case the deviations from the exact results are noticeable even for the highest degree of precision studied. The calculated spectrum is broader than the exact one and the calculated velocity correlation function decays more rapidly than the exact velocity correlation function. The excellent accuracy at short times of the calculated velocity correlation function from imaginary-time data hav-

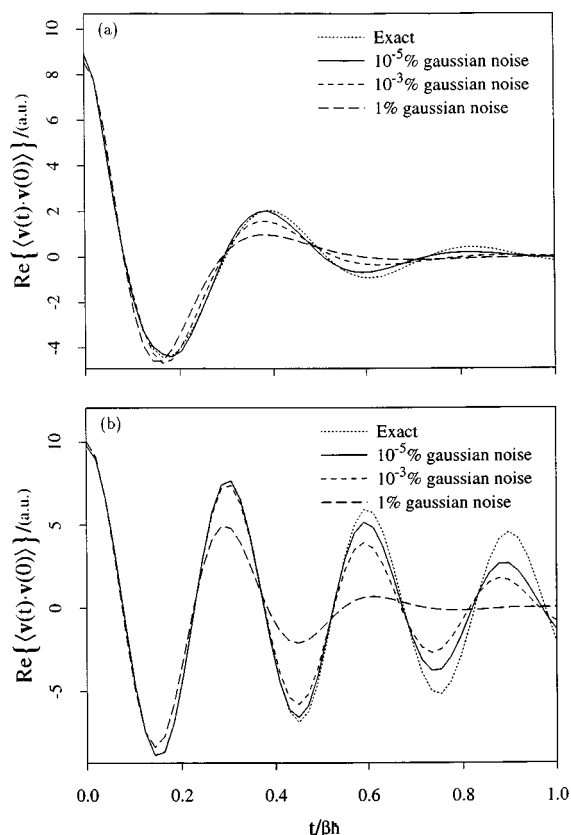


FIG. 4. The real part of the velocity correlation functions of the harmonic oscillator linearly coupled to a bath of harmonic oscillators with (a)  $f=1$  and (b)  $f=0.2$ , calculated from the spectra of Fig. 3, compared with the exact velocity correlation functions from Fig. 2(b).

ing only two significant figures is, however, remarkable.

For the high damping case the bias introduced by the numerical maximum entropy analytic continuation method seems to be less important, even though at least four significant figures in the input is necessary to achieve satisfactory accuracy.

It should be stressed that one should not expect the results from imaginary-time data generated by a PIMC computer simulation to be better than the ones given here because the calculated imaginary-time data are also affected by systematic errors.

The effect of the systematic errors caused by the discretization of path integral are investigated next.

In numerical path integral calculations by the PIMC method, the discretization with a finite number  $p$  of time slices of the path integral introduces an error in the calculated averages that decreases with increasing  $p$ . In the present application the error due to the finiteness of  $p$  can be obtained exactly by comparing Eqs. (38)–(39) and (41). To avoid the summation of the infinite series, the exact displacement imaginary-time correlation function can be calculated by Eq. (18) by using the exact absorption cross section  $\sigma(\omega)$  from Eq. (14). For both values of the parameter  $f$ , an accuracy up to three significant figures is achieved for  $p=256$ . The values of  $R^2(-i\tau)_{(p)}$  from Eq. (41) with  $10^{-4}\%$  noise have been used as input for the maximum entropy analytic continuation method and the resulting absorption

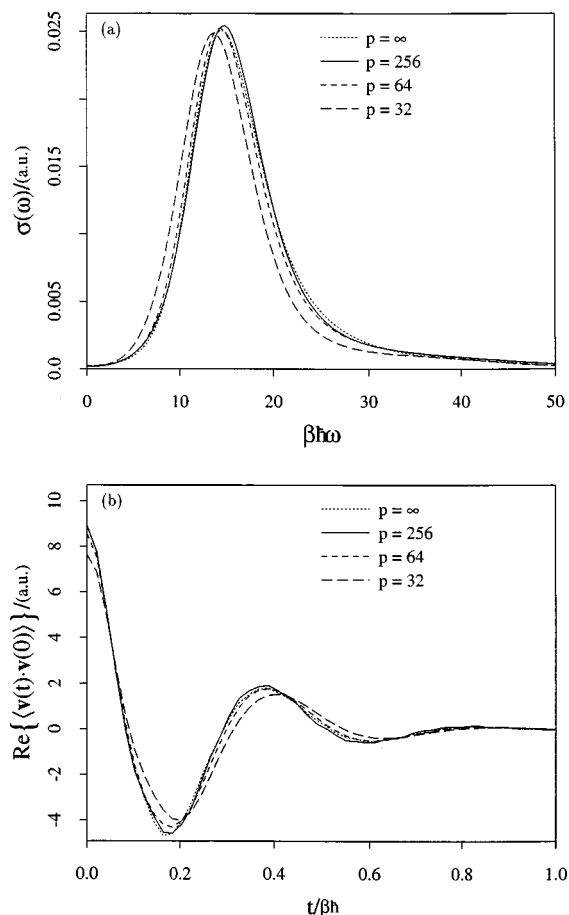


FIG. 5. (a) The absorption cross sections and (b) the real part of the velocity correlation functions of the harmonic oscillator linearly coupled to a bath of harmonic oscillators for  $f=1$ , calculated by maximum entropy inversion of the imaginary-time displacement correlation functions for finite  $p$ , compared to the maximum entropy spectra and velocity correlation functions obtained from the exact imaginary-time data.

cross sections and velocity correlation functions are shown for the high damping case in Fig. 5. Similar results have been obtained for the low damping case. In Fig. 5 the quantities calculated for finite  $p$  are compared to the corresponding ones calculated previously by the maximum entropy method for  $p=\infty$ . The effects of the discretization error are insignificant compared to the bias introduced by the maximum entropy method. In the PIMC simulations, described next, we set  $p=256$  which provides results very close to the  $p=\infty$  limit.

A PIMC simulation based on the action in Eq. (34) with  $p=256$  and  $V(x)=m\omega_0x^2/2$ , where  $m=1$  a.u. and  $\omega_0=20$  a.u., and  $\beta=1$  a.u. is performed for the two values of the parameter  $f$  in Eq. (42). The quantum mechanical imaginary-time dynamical friction kernel  $\Gamma(\tau)$  is calculated using Eq. (32) where  $J_b(\omega)$ , the spectral function of the bath modes, is the cosine transform of the classical dynamical friction kernel  $\zeta(t)$  given in Eq. (42). The configurations of the quantum cyclic polymer are sampled by the staging method<sup>47,30</sup> based only on the kinetic energy part of the action. More efficient sampling methods can be devised based on the quadratic part of the potential<sup>48,49</sup> and, as we have shown, the action in Eq. (34) could be completely diagonal-

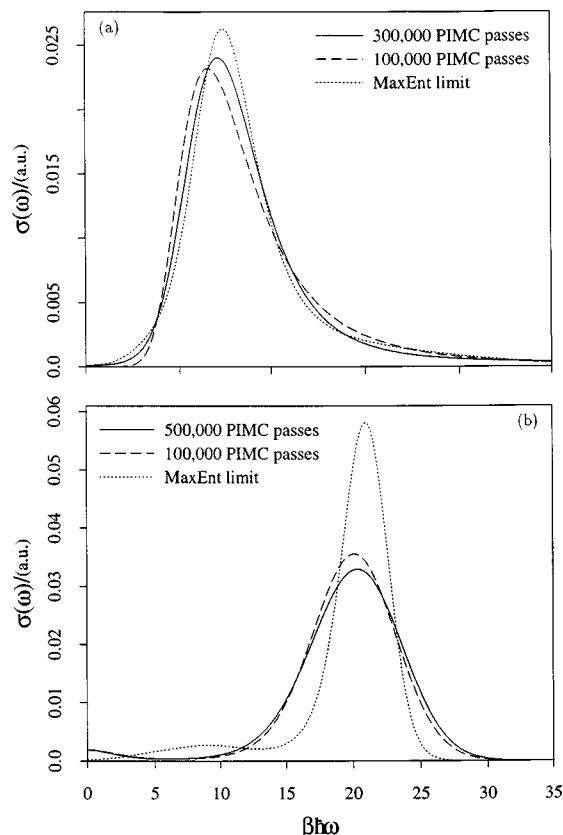


FIG. 6. The absorption cross sections of the harmonic oscillator linearly coupled to a bath of harmonic oscillators for (a)  $f=1$  and (b)  $f=0.2$ , calculated by maximum entropy inversion of the imaginary-time displacement correlation functions from PIMC simulations, compared to the maximum entropy spectra from Fig. 3 corresponding to  $10^{-5}\%$  Gaussian noise.

ized in the form of a product of Gaussian functions so that the sampling would be reduced just to the generation of Gaussian random numbers. We, however, prefer to test the maximum entropy analytic continuation method using imaginary-time data from primitive PIMC calculations because they can be applied with ease to a wide variety of problems such as a particle in a double-well potential. The tests reported here for an harmonic oscillator should be, therefore, equally valid for more complicated systems, such as an anharmonic oscillator coupled to other explicit degrees of freedom.

The main difference between the mock data set considered previously, to which Gaussian noise is added, and the one produced by the simulation is that the latter data has cross correlation, that is, the fluctuations of the imaginary-time data at different imaginary-time slices are correlated. In this case it is necessary to perform an uncorrelation procedure of the data as the maximum entropy method assumes uncorrelated data for input.<sup>26,28,27</sup>

The calculated absorption cross sections for the two cases examined are shown in Fig. 6. They are compared with the absorption spectra obtained by the numerical maximum entropy method from the exact data with seven significant digits (see Fig. 3). This comparison points out the effect of the statistical uncertainties that are contained in the imaginary-time data generated by the PIMC simulation. The

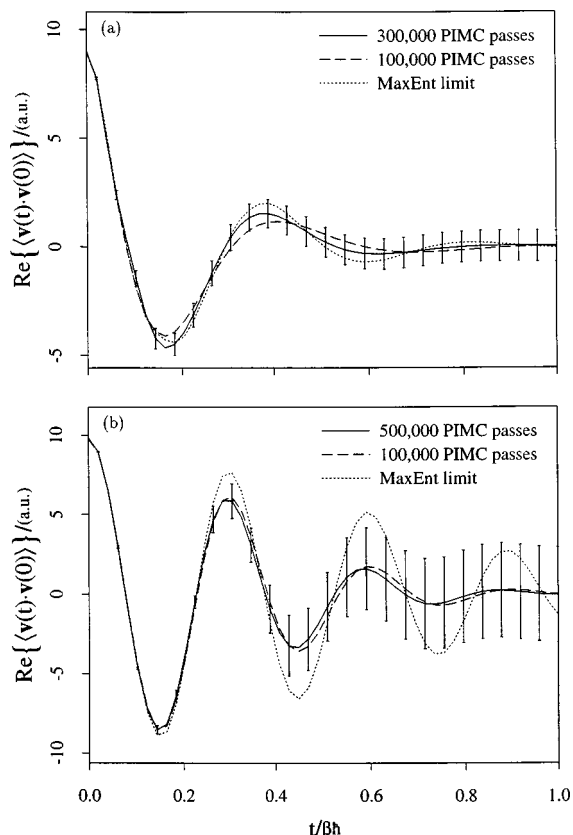


FIG. 7. The real part of the velocity correlation functions of the harmonic oscillator linearly coupled to a bath of harmonic oscillators for (a)  $f=1$  and (b)  $f=0.2$ , calculated from the spectra of Fig. 6, compared to the maximum entropy velocity correlation functions from Fig. 4 corresponding to  $10^{-5}\%$  Gaussian noise.

corresponding velocity correlation functions are shown in Fig. 7. The results for the high damping case ( $f=1$ ) from a 300 000-passes PIMC simulation are equivalent to mock data with  $10^{-3}\%$  noise. The 300 000-passes PIMC simulation provides a sensible improvement over a simulation three times shorter. The results for the low damping case show a different behavior: A 100 000-passes PIMC simulation provides results equivalent to mock data with 0.1% noise and a simulation five times longer does not seem to improve the quality of the results even though the correlation analysis shows that the statistical errors on the uncorrelated data decreases by a factor of  $\sqrt{5}$  as expected.

By comparing Fig. 3(a), Fig. 5(a), and 6(a), we notice that for the high damping case there is a good quantitative agreement between the maximum entropy absorption cross sections calculated from the PIMC data and the exact absorption cross section. Most of the deviation is due to the bias introduced by the numerical procedure used to implement the maximum entropy analytic continuation method. This is also true for the calculated velocity autocorrelation function.

In the low damping case, instead, we notice that the statistical uncertainties of the PIMC data are also of relevance because the convergence of the absorption cross section with respect to the PIMC simulation length seems to be very slow. In addition, the maximum entropy bias [see Figs. 3(b) and 6(b)] is noticeably more pronounced than in the

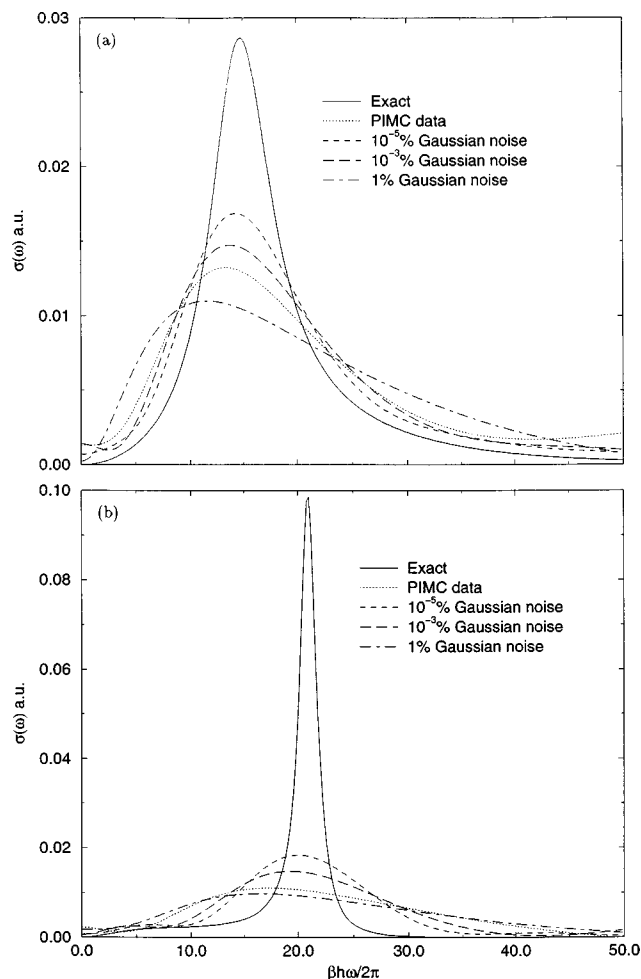


FIG. 8. (a) High damping case ( $f=1$ ) and (b) low damping case ( $f=0.2$ ): the exact and SVD absorption cross sections obtained by analytic continuation of PIMC data and analytic continuation of the exact imaginary-time correlation function with various amounts of added random Gaussian noise.

high damping case. This, again, may be understood in terms of the width of the absorption band that in the high damping case is several times the estimated maximum entropy frequency resolution,<sup>27</sup>  $\beta\hbar\Delta\omega \approx \pi$ , whereas the bandwidth in the low damping case is very close to the maximum entropy frequency resolution. We expect, therefore, the latter to be more difficult to reproduce by any numerical analytic continuation method.

The real-time dynamics for the low damping case is also more difficult to study because, in this case, the dynamics of the oscillator is characterized by a longer timescale (corresponding to the vibrational relaxation rate). In the high damping case, instead, most of the dynamical properties are determined by the short-time dynamics for  $t < \beta\hbar$  that is within the time domain appropriate for applying analytic continuation methods.

## B. Singular value decomposition inversion

We have applied the SVD method to reconstruct the absorption spectrum of a harmonic oscillator bilinearly coupled to a harmonic bath from the imaginary-time displacement correlation function; we have considered the ‘‘high damp-

ing’’ ( $f=1$ ) and the ‘‘low damping’’ ( $f=0.2$ ) cases. As in the case of the maximum entropy method, we have first applied SVD to the exact imaginary-time data, to which Gaussian random noise has been added; the relative amplitude of the noise has been gradually decreased from 1% to  $10^{-5}\%$ . The exact imaginary-time data are calculated on the grid  $\tau_i = i\beta\hbar/256$  for  $i=1, \dots, 128$ , and the frequency grid for the calculation of the absorption spectra is comprised of 250 points on the interval  $0 < \omega < 50$  a.u. for the low damping case and  $0 < \omega < 100$  a.u. for the high damping case. The results for the absorption spectra calculated from Eq. (27) are shown in Fig. 8(a) and 8(b). It is immediately clear that the resolution of the SVD method is much poorer compared to the MEM results for the same level of random noise. Even for the lowest level of noise ( $10^{-5}\%$ ) the results are far from being converged to the exact answer, especially in the low damping case. Presumably, this poor resolution is due to the additional ‘‘positivity constraint’’ which we had to impose on the SVD solution. We have also applied the SVD approach to the simulated PIMC data, in which case a certain amount of the cross correlation between the different imaginary-time slices is present. The results are also plotted in Fig. 8; they fall in between the results obtained with the artificial noise of amplitude 1% and  $10^{-3}\%$ ; this is consistent with the magnitude of statistical error in the simulation data.

## VIII. CONCLUSIONS

Path integral Monte Carlo (PIMC) simulations provide a general prescription for simulating quantum fluids and have been very useful for exploring the thermodynamics and structure of quantum fluids and solute-solvent systems such as the solvated electron. Unfortunately, these methods cannot be used to directly simulate dynamics because of the notorious ‘‘sign problem.’’ There is a clear need for methods to determine quantum time-correlation functions and transport. Since PIMC methods allow the determination of imaginary-time correlation functions, and because real-time correlation functions are analytic continuations of imaginary-time correlation functions, it is important to assess methods such as SVD and maximum entropy, which provide numerical analytical continuations. Although we have already used these methods to predict dynamics in solvated electron systems<sup>26–28</sup> and in vibronic transitions in solvated molecules,<sup>29</sup> it is important to use them on systems for which the exact quantum dynamics is known. This will allow direct assessment of the accuracy of these numerical schemes to be made. Unfortunately, very few exactly solvable systems are known. In this paper we study one such system: the vibrational relaxation of a harmonic oscillator coupled to a harmonic bath. The numerical analytical continuation methods studied are found to be accurate only at short times. They are, therefore, not applicable to slow relaxation processes.

We have used two numerical analytical continuation methods to analyze the relaxation dynamics of a harmonic oscillator bilinearly coupled to a bath of harmonic oscillators. We have obtained the real-time velocity correlation functions and the optical absorption cross sections of the oscillator from the corresponding imaginary-time displace-

ment correlation functions. The result of the computations have been compared to the available analytical results. We find good agreement between the calculated and analytical results when the relaxation time of the velocity correlation function of the tagged oscillator is short (high damping case). The instability of the numerical analytical continuation methods for larger real times is the cause of the disagreement between calculated and analytical results for longer relaxation times (low damping case).

In general, we find that the maximum entropy analytic continuation method, which enforces positivity of the absorption cross section, performs better than the singular value analytical continuation method. One possible way to improve the performance of the SVD method is by reconstructing the difference between the quantum mechanical spectrum and the one obtained from centroid molecular dynamics. This difference can alternate in sign, and the SVD method can be applied without imposing the positivity constraint. Hence, higher resolution can be expected. This approach will be the subject of future investigations.

To study the origin of the discrepancy between calculated and analytical results, we have performed the computations on imaginary-time data from two sources: (i) from exact imaginary-time correlation functions with added Gaussian random noise; and (ii) from imaginary-time correlation functions from path integral Monte Carlo simulations. We find that the noise on the data and the discretization errors introduced by the implementation of the analytic continuation procedures are the major source of discrepancies between calculated and exact results. For the low damping case, the precision necessary to achieve satisfactory agreement with the exact results is probably beyond the finite arithmetics used to perform the computations. The present finding provides useful guidelines for future applications of numerical analytical continuations methods to path integral Monte Carlo data.

<sup>1</sup>J. C. Tully, *J. Chem. Phys.* **93**, 1061 (1990).

<sup>2</sup>D. F. Coker, in *Computer Simulations in Chemical Physics*, edited by M. P. Allen and D. J. Tildesley (Kluwer Academic, Dordrecht, 1993), pp. 315–377.

<sup>3</sup>W.-S. Sheu and P. J. Rossky, *J. Am. Chem. Soc.* **115**, 7729–7735 (1993).

<sup>4</sup>L. Xiao and D. F. Coker, *J. Chem. Phys.* **102**, 1107 (1995).

<sup>5</sup>S. Hammes-Schiffer and J. C. Tully, *J. Chem. Phys.* **101**, 4657 (1994).

<sup>6</sup>S. Hammes-Schiffer, *J. Chem. Phys.* **105**, 2236 (1996).

<sup>7</sup>P. J. Rossky and J. Schnitker, *J. Phys. Chem.* **92**, 4277–4285 (1988).

<sup>8</sup>F. J. Webster, J. Schnitker, M. S. Friedrichs, F. A. Friesner, and P. J. Rossky, *Phys. Rev. Lett.* **66**, 3172 (1991).

<sup>9</sup>J. S. Bader and B. J. Berne, *J. Chem. Phys.* **100**, 8359 (1994).

<sup>10</sup>S. A. Egorov and B. J. Berne, *J. Chem. Phys.* **107**, 6050–6061 (1997).

<sup>11</sup>S. A. Egorov, Eran Rabani, and B. J. Berne, *J. Chem. Phys.* **108**, 1407–1422 (1998).

<sup>12</sup>K. Blum, *Density Matrix Theory and Applications* (Plenum, New York, 1981).

<sup>13</sup>A. G. Redfield, *Adv. Magn. Reson.* **1**, 1 (1965).

<sup>14</sup>W. T. Pollard, A. K. Felts, and R. A. Friesner, *Adv. Chem. Phys.* **93**, 77 (1996).

<sup>15</sup>S. A. Egorov and J. L. Skinner, *J. Chem. Phys.* **105**, 7047–7058 (1996).

<sup>16</sup>F. E. Figuerido and R. M. Levy, *J. Chem. Phys.* **97**, 703 (1992).

<sup>17</sup>H. Gai and G. A. Voth, *J. Chem. Phys.* **99**, 740 (1993).

<sup>18</sup>B. J. Berne and D. Thirumalai, *Annu. Rev. Phys. Chem.* **37**, 401–424 (1986).

<sup>19</sup>V. S. Filinov, *Nucl. Phys. B* **271**, 717 (1986).

<sup>20</sup>N. Makri, *Comput. Phys. Commun.* **63**, 389–414 (1991).

<sup>21</sup>M. Topaler and N. Makri, *J. Chem. Phys.* **97**, 9001 (1992).

<sup>22</sup>M. Topaler and N. Makri, *J. Phys. Chem.* **100**, 4430 (1996).

<sup>23</sup>G. A. Voth, *Adv. Chem. Phys.* **93**, 135 (1996).

<sup>24</sup>G. Baym and D. Mermin, *J. Math. Phys.* **2**, 232 (1960).

<sup>25</sup>D. Thirumalai and B. J. Berne, *Comput. Phys. Commun.* **63**, 415–426 (1991).

<sup>26</sup>E. Gallicchio and B. J. Berne, *J. Chem. Phys.* **101**, 9909–9918 (1994).

<sup>27</sup>E. Gallicchio and B. J. Berne, *J. Chem. Phys.* **105**, 7064–7078 (1996).

<sup>28</sup>Emilio Gallicchio, Ph.D. thesis, Columbia University, Graduate School of Arts and Sciences, New York, NY, 1996.

<sup>29</sup>S. A. Egorov, E. Gallicchio, and B. J. Berne, *J. Chem. Phys.* **107**, 9312 (1997).

<sup>30</sup>M. E. Tuckerman, B. J. Berne, G. J. Martyna, and M. L. Klein, *J. Chem. Phys.* **99**, 2796 (1993).

<sup>31</sup>M. Tuckerman and B. J. Berne, *J. Chem. Phys.* **98**, 7301 (1993).

<sup>32</sup>A. Nitzan, S. Mukamel, and J. Jortner, *J. Chem. Phys.* **63**, 200–207 (1975).

<sup>33</sup>S. A. Egorov and J. L. Skinner, *J. Chem. Phys.* **106**, 1034–1040 (1996).

<sup>34</sup>B. J. Berne, in *Physical Chemistry, An Advanced Treatise*, edited by H. Eyring (Academic, New York, 1967–75), Vol. III B, Chap. 9.

<sup>35</sup>J. E. Straub, M. Borkovec, and B. J. Berne, *J. Phys. Chem.* **91**, 4995–4998 (1987).

<sup>36</sup>B. J. Berne, M. E. Tuckerman, J. E. Straub, and A. L. R. Bug, *J. Chem. Phys.* **93**, 5084 (1990).

<sup>37</sup>M. Jarrell and J. E. Gubernatis, *Phys. Rep.* **269**, 133 (1996).

<sup>38</sup>J. Skilling, in *Maximum Entropy and Bayesian Methods*, edited by J. Skilling (Kluwer Academic, Dordrecht, 1989).

<sup>39</sup>S. F. Gull, in *Maximum Entropy and Bayesian Methods*, edited by J. Skilling (Kluwer Academic, Dordrecht, 1989).

<sup>40</sup>C. E. Creffield, E. G. Klepfish, E. R. Pike, and S. Sarkar, *Phys. Rev. Lett.* **75**, 517 (1995).

<sup>41</sup>W. H. Press, B. P. Flannery, S. A. Teukolsky, and W. T. Vetterling, *Numerical Recipes* (Cambridge University Press, Cambridge, 1986).

<sup>42</sup>M. Bertero, P. Brianzi, E. R. Pike, and L. Rebolia, *Proc. R. Soc. London, Ser. A* **415**, 257 (1988).

<sup>43</sup>R. P. Feynman, *Statistical Mechanics* (Addison-Wesley, New York, 1972).

<sup>44</sup>D. Chandler, in *Liquids, Freezing and Glass Transition*, edited by D. Levesque, J. P. Hansen, and J. Zinn-Justin (Elsevier Science, New York, 1990).

<sup>45</sup>M. F. Herman, E. J. Bruskin, and B. J. Berne, *J. Chem. Phys.* **76**, 5150–5155 (1982).

<sup>46</sup>J. E. Straub, M. Borkovec, and B. J. Berne, *J. Chem. Phys.* **89**, 4833–4847 (1988).

<sup>47</sup>E. L. Pollock and D. M. Ceperley, *Phys. Rev. B* **30**, 2555–2568 (1984).

<sup>48</sup>R. A. Friesner and R. M. Levy, *J. Chem. Phys.* **80**, 4488–4495 (1984).

<sup>49</sup>C. H. Mak and H. C. Andersen, *J. Chem. Phys.* **92**, 2953–2965 (1990).